Mineralium Deposita (2025) 60:1397–1408
https://doi.org/10.1007/s00126-025-01350-2

ARTICLE

Apatite as a pathfinder to tin mineralisation: prospects and caveats

Martin F. Mangler[1,3] · Nicholas J. Gardiner[1] · Dominic Skeat[1] · Nick M. W. Roberts[2] · Simon Tapster[2]

Received: 4 September 2024 / Accepted: 28 January 2025 / Published online: 13 February 2025

Abstract

Granite-related mineral deposits are major primary sources of the critical metals tin (Sn) and lithium (Li). The utility of accessory minerals such as zircon and apatite as pathfinders to these ore deposits has been a subject of great interest in recent years, with a number of geochemical discriminants having been developed to distinguish barren from metal-fertile and mineralised intrusions. Here, we study the potential of apatite as an indicator mineral for tin and lithium mineralisation using a compilation of published apatite trace element data as well as new data for the mineralised Cornubian batholith and barren Bhutanese leucogranites. Critical examination of common geochemical discriminants tracing magma fractionation and redox conditions (Mn, Eu/Eu*, La/Yb_N and Sr/Y) reveals large and overlapping data scatter for both barren and Sn-fertile intrusions. This calls into question the utility of these petrogenetic indicators to pinpoint tin metallogeny. Instead, *prima facie* metal concentrations directly related to tin mineralisation (i.e., Sn and Li) are consistently elevated in apatite from fertile and mineralised intrusions. Based on our data compilation, Li and Sn concentrations in apatite are the most robust indicators for Sn (and Li) mineralisation, and we encourage the community to include Li and Sn in their analytical routines to further test these observations and explore their implications for tin metallogeny.

Keywords Tin mineralisation · Apatite · Trace elements · LA-ICP-MS · Exploration

Introduction

Apatite ($Ca_5(PO_4)_3(OH, F,Cl)$) is a common accessory mineral in magmas across the compositional spectrum. Its stability is primarily controlled by P concentrations in the magma, and it often appears early in the crystallisation sequence of granites (Hoskin et al. 2000; Piccoli and Candela 2002; Broska et al. 2004; Macdonald et al. 2013; Miles et al. 2013; Zhang et al. 2021). Apatite can accommodate a range of key minor and trace elements such as REE, Sr, U, Pb, and Th (Belousova et al. 2002; Mao et al. 2016); in particular, high apatite-melt partition coefficients for REE, Sr, and Y ($D_{ap/melt}$ ~3–10; Prowatke and Klemme 2006) mean that apatite exerts significant control on the trace element budget of a magma during differentiation. Conversely, its wide stability field and compositional range make apatite a potentially powerful proxy through which to study evolving magma conditions and dynamics (Sha and Chappell 1999; Miles et al. 2013, 2014; Stock et al. 2018; Li et al. 2021; Lormand et al. 2024; Xu et al. 2024). Moreover, apatite trace element compositions have been used to discriminate between different rock types, such as lherzolites, carbonatites, mafic rocks, granitoids, granite pegmatites, and iron oxides (Belousova et al. 2002), as well as S-type and I-type granites (Sha and Chappell 1999), highlighting the utility of apatite in provenance studies.

Apatite is also a common accessory mineral in granite-hosted hydrothermal ore deposits, and hence Belousova et al. (2002) highlighted the potential use of apatite as a resistate indicator mineral (RIM) in exploration for critical metals thanks to its widespread occurrence, wide stability field, relative resistance to weathering and surface processes, and ability to incorporate commodity elements such as Ni, Cu, Zn, and As. Since then, discriminant analysis of

Editorial handling: B. Lehmann

✉ Martin F. Mangler
M.F.Mangler@soton.ac.uk

[1] School of Earth & Environmental Sciences, University of St Andrews, St. Andrews KY16 9TS, UK

[2] Geochronology and Tracers Facility, British Geological Survey, Nottingham NG12 5GG, UK

[3] School of Ocean and Earth Science, University of Southampton, Southampton SO14 3ZH, UK

apatite has been used to distinguish magmatic-hydrothermal mineral deposits from unmineralised rocks using a combination of Mg, V, Mn, Sr, Y, REE, Pb, Th, and U concentrations in apatite (Mao et al. 2016). The same authors also put forward characteristic apatite compositions for different mineralisation styles, including alkalic porphyry Cu-Au deposits, porphyry Cu±Mo±Au deposits, and Kiruna-type iron oxide apatite deposits (Mao et al. 2016). Similarly, Ding et al. (2015) distinguished between Cu-Pb-Zn porphyries and W-Sn-bearing granites by tracing the geochemical signatures of their respective magmatic sources (i.e., I-type vs. S-type granites) in apatite.

Due to efforts to develop new metallogenic models for 'lithophile' granite-related magmatic-hydrothermal deposits, which host Sn, Li and other critical metals such as W and Ta, there has been growing interest in the use of accessory minerals as fertility indicators. The aim is to utilise accessory minerals to discriminate barren from metal-fertile rocks and ultimately to establish them as reliable pathfinders for new mineral deposits. Hence, a small number of studies have recently examined the utility of apatite to explore for Sn mineralisation (Azadbakht et al. 2018; Guo et al. 2022; Li et al. 2022). These studies analysed trace elements in magmatic apatite from granitoids associated with Sn-mineralisation and suggested that Sn-fertile intrusions can be distinguished from barren magmas by their high Mn, Fe, Li and Sn concentrations and their low LREE/HREE and Eu/Eu* ratios. However, these studies focused on specific case studies, and to date, no global compilation of trace element characteristics of apatite associated with Sn deposits has been produced.

Here, we compile published trace element data for apatite from barren and Sn-fertile igneous rocks, and we complement this compilation with new apatite trace element data from Sn-mineralised units in the Cornubian batholith (SW England), as well as for barren 'Himalayan'-style leucogranites from Bhutan. We use this dataset to assess the fidelity of previously suggested trace element signatures in apatite to distinguish barren from Sn-fertile rocks, with the aim of identifying the geochemical discriminants which most robustly point towards tin mineralisation.

Geochemical discriminants in apatite

Geochemical discriminants developed for apatite are empirical in nature and aim to assess magmatic source, degree of fractionation, and oxidation state, since these petrogenetic constraints are considered to control the potential for granite-hosted mineralisation (Blevin and Chappell 1992; Blevin et al. 1996; Černý et al. 2005; Gardiner et al. 2017). In particular, tin mineralisation is typically associated with highly fractionated, reduced granites derived from melting of crustal sediments (S-type; Taylor 1979; Lehmann 1982, 2021; Taylor and Wall 1992; Romer and Kroner 2015, 2016; Gardiner et al. 2024). Hence, the geochemical tracers proposed as pathfinders to tin mineralisation are those that pinpoint such high degrees of fractionation and low oxygen fugacity:

(1) **Sr** and **Y** in apatite are often used in combination to trace the degree of melt fractionation: Whilst Sr generally decreases during melt evolution due to plagioclase fractionation, Y is progressively enriched in the melt (Belousova et al. 2002). These trends in melt composition are thought to be reflected in apatite compositions. However, high melt (and hence apatite) Sr/Y ratios may also reflect a high Sr/Y parental magma source, melting of a garnet-bearing source, or amphibole-dominated fractional crystallisation (Moyen 2009; Nathwani et al. 2020).

(2) **La/Yb_N** and other ratios reflecting the slope of REE patterns also trace the degree of magma fractionation: whilst apatite generally shows negative REE slopes, LREE/HREE ratios decrease by about two orders of magnitude during fractionation from primitive to highly evolved compositions; in pegmatites, REE slopes tend to be positive (i.e., LREE/HREE < 1; Belousova et al. 2002). A primary reason for the LREE depletion is crystallisation of monazite or allanite, which preferentially incorporate LREE (Tepper and Kuehner 1999; Miles et al. 2014; Li et al. 2022) thereby passively enriching HREE despite their slightly lower ap-melt partition coefficients (Prowatke and Klemme 2006). Similar to all fractionation proxies, individual apatite La/Yb_N ratios therefore depend on the crystallising assemblage and the relative timing of apatite crystallisation.

(3) **Eu anomalies (Eu/Eu*, where $Eu^* = (Sm_N \cdot Gd_N)^{1/2}$)** are ubiquitously used proxies for magma fractionation in apatite (Belousova et al. 2002; Jia et al. 2020; Nathwani et al. 2020): negative Eu anomalies will increase during melt evolution due to plagioclase fractionation, which controls Eu/Eu* in apatite. As a result, the most evolved rocks are characterised by apatite with extreme Eu/Eu* <0.1 (Belousova et al. 2002). In addition, Miles et al. (2014) point out that Eu^{3+} is more compatible in apatite than Eu^{2+} (Prowatke and Klemme 2006), and negative Eu anomalies could therefore, in theory, reflect reducing magma conditions. However, Eu/Eu* in apatite is only a useful recorder of magmatic oxygen fugacity if it can be shown to be an early crystallising phase, otherwise the effect of feldspar fractionation dominates Eu/Eu* (Bromiley 2021). In contrast to zircon (Gardiner et al. 2017), Ce anomalies are rare in apatite (Belousova et al. 2002; Miles et al. 2014; Bromiley 2021).

(4) **Mn** is another element that has been argued to reflect magmatic conditions: manganese concentrations generally increase in the melt during fractionation, and increasing Mn concentrations in apatite are therefore often interpreted to reflect melt evolution (similar to Y); **Fe** displays analogous trends. On the other hand, Belousova et al. (2002) suggested that Mn in apatite is redox sensitive, and Miles et al. (2014) argued that Mn in apatite may be used as a redox proxy in silicic melts. However, an experimental study by Stokes et al. (2019) found that Mn partitioning between apatite and silicate melt is not dependent on oxygen fugacity, and that Mn^{2+} is the dominant species irrespective of redox conditions. Instead, Stokes et al. (2019) conclude that Mn partitioning into apatite is primarily controlled by the degree of melt polymerisation.

The utility of the above discriminants relies on the implicit assumption that extreme fractionation of reduced S-type granites is sufficient to concentrate Sn enough to form mineralised deposits (Lehmann 2021). However, as outlined above, a key commonality of such petrogenetic discriminants is that they are sensitive to several magmatic process and variables, and hence their petrogenetic significance is often ambiguous. Other discriminants target volatile compositions (i.e., **F** and **Cl** concentrations in apatite), but most studies find overlapping data and generally extreme enrichment in F and depletion in Cl (Ding et al. 2015; Mao et al. 2016; Azadbakht et al. 2018; Guo et al. 2022; Li et al. 2022). Halogen concentrations will therefore not be further considered in this study.

Less commonly, concentrations of the commodity metals themselves– e.g., **Sn** and **Li** concentrations– are reported for apatite. Recent studies indicate that apatite in igneous rocks associated with Sn mineralisation displays elevated Sn and Li concentrations (Azadbakht et al. 2018; Li et al. 2020; Guo et al. 2022), though to date there is not enough data to substantiate this finding. To this end, we analysed an additional 74 apatite crystals from barren and Sn-fertile rocks ($n=411$ analyses), with particular focus on Sn and Li concentrations.

Materials and methods

We compiled a dataset of published and new apatite trace element data obtained using laser ablation inductively coupled plasma mass spectrometry (LA-ICP-MS), with particular focus on Sn and Li concentrations in apatite. We categorised the apatite data into (i) *barren*: magmatic apatite from Sn-infertile intrusions; (ii) *Sn-fertile*: magmatic apatite from unmineralised domains of intrusions associated with tin mineralisation. These apatite crystals typically show no evidence for hydrothermal alteration; (iii) *Sn-mineralised*: apatite from altered, cassiterite-bearing regions of intrusions (including pegmatites, aplites and greisens). These apatite crystals have typically been affected by variable degrees of hydrothermal alteration and some may be of hydrothermal origin.

In total, the dataset includes 343 datapoints for barren, 188 datapoints for Sn-fertile, and 136 datapoints for Sn-mineralised apatite. In addition, we compiled published apatite trace element data from Cu-fertile intrusions for reference ($n=460$). The compiled data (Table 1; ESM 1) was screened for outliers using a 3SD criterion, and results below detection limit are considered a zero result.

Published data

We compiled apatite trace element data from four studies (Azadbakht et al. 2018; Guo et al. 2022; Li et al. 2022; Ge et al. 2024; Table 1). Apatite in the selected studies is described as magmatic in all cases, and they are either from barren or Sn-fertile intrusions. The literature compilation includes 109 apatite datapoints from Sn-fertile intrusions (three biotite granites from the Geiju Sn polymetallic district, China, Li et al. 2022; two biotite granites from the Dachang Sn polymetallic district, China, Guo et al. 2022; three biotite granites and one syenogranite from Acadia, Canada, Azadbakht et al. 2018) and 148 apatite datapoints from barren intrusions (one gabbro, one monzonite, and three biotite granites from the Dachang Sn polymetallic district, China, Guo et al. 2022; one gabbro-diorite from the Zhuxiling tungsten deposit, China, Ge et al. 2024; and four biotite granites from Acadia, Canada, Azadbakht et al. 2018). For comparison, we also compiled published data from magmatic apatite associated with Cu mineralisation ($n=460$; Yang et al. 2018; Nathwani et al. 2020; Pan et al. 2020, 2021; Parra-Avila et al. 2022).

Additional Samples

To ensure the representativeness of our global study on apatite as a pathfinder to tin mineralisation, we performed additional analyses of apatite crystals from the fertile and mineralised portions of the Cornubian batholith as well as from three barren leucogranites from Bhutan (Table 1; ESM 2 and 3). The Cornubian batholith samples include two Sn-fertile granites: a biotite granite (CW 02; $n=38$) from the G3 series, and a G5 topaz granite (Tregonning granite; CW TREG; $n=41$) (Simons et al. 2016). In addition, apatite from an Sn-mineralised greisenised granite of the G2 muscovite series (Cligga Head; CW 12; $n=100$), and from a mineralised aplite from the G5 topaz series (Meldon Aplite;

Table 1 Summary of data compiled for this study

Study area	Unit	Identifier	Rock type	Category	n_{ap}	Reference
Geiju, China	Beipaotai	BPT-1	Granite	fertile	24	Li et al. 2022
Geiju, China	Masong	MLG-2	Granite	fertile	24	Li et al. 2022
Geiju, China	Longchahe	LCH-12	Granite	barren	25	Li et al. 2022
Geiju, China	Baishachong	BSC-16	Granite	barren	24	Li et al. 2022
Geiju, China	Shenxianshui	SXS-2	Granite	barren	25	Li et al. 2022
Geiju, China	Laoka	XALK-1	Granite	fertile	24	Li et al. 2022
Geiju, China	Jiasha	JS-5	Monzonite	barren	25	Li et al. 2022
Geiju, China	Longchahe	LCH-14	Gabbro	barren	22	Li et al. 2022
Zhuxiling, China	Zhuxiling	ZXL1	Gabbro-diorite	barren	23	Ge et al. 2024
New Brunswick, Canada	Lost Lake	WX85-NB-161	Granodiorite	barren	1	Azadbakht et al. 2018
New Brunswick, Canada	Mount Douglas	WX85-NB-198	Granite	barren	1	Azadbakht et al. 2018
New Brunswick, Canada	Mount Douglas	WX85-NB-220	Granite	barren	1	Azadbakht et al. 2018
New Brunswick, Canada	Mt LaTour	WX85-NB-254	Granite	barren	1	Azadbakht et al. 2018
New Brunswick, Canada	Beech Hill	WX85-NB-188	Granite	fertile	1	Azadbakht et al. 2018
New Brunswick, Canada	Utopia	WX85-NB-189	Syenogranite	fertile	1	Azadbakht et al. 2018
New Brunswick, Canada	Trout Lake	WX85-NB-225	Leucogranite	fertile	1	Azadbakht et al. 2018
New Brunswick, Canada	Dungarvon	WX85-NB-226	Granite	fertile	1	Azadbakht et al. 2018
Dachang, China	Dachang	ZK10-1-21	Granite	fertile	20	Guo et al. 2022
Dachang, China	Dachang	ZK10-1-32	Granite	fertile	13	Guo et al. 2022
Cornwall, UK	Dartmoor (G3)	CW 02	Granite	fertile	38	This study
Cornwall, UK	Cligga Head (G2)	CW 12	Granite	mineralised	100	This study
Cornwall, UK	Meldon (G5)	CW MELAP	Aplite	mineralised	36	This study
Cornwall, UK	Tregonning (G5)	CW TREG	Granite	fertile	41	This study
Himalayan leucogranites	Gasa, Bhutan	NR1514	Leucogranite	barren	74	This study
Himalayan leucogranites	Gasa, Bhutan	NR1515	Leucogranite	barren	72	This study
Himalayan leucogranites	Gasa, Bhutan	NR1516	Leucogranite	barren	49	This study

CW MELAP; $n=36$) were analysed. The barren Bhutanese leucogranites ($n=195$) are ~17−15 Ma pure S-type granites related to melting of pelitic protoliths during the Himalayan orogeny (Hopkinson et al. 2017). Brief sample descriptions and sampling locations are provided in ESM 3. Apatite crystals in barren and Sn-fertile rocks are generally homogeneous and show no signs of alteration, whereas some crystals from mineralised units are partially altered (ESM 3).

Analytical methods

Apatite crystals for new analyses were separated from sieved whole rock samples (<250 µm fractions) via heavy liquid and magnetic separation before being mounted in epoxy resin. The mounts were imaged and analysed using a Jeol JXA-iSP100 electron microprobe and Jeol JSM-IT200 SEM at the University of St Andrews, UK, to aid targeting suitable crystals. Despite the complex nature of some apatite grains separated from the mineralised samples (ESM 3), we only placed ablation spots within the crack-free pristine regions of each grain. Laser ablation ICP-MS analyses were conducted at the British Geological Survey Keyworth, UK using an ESL 193 nm ImageGeo excimer laser ablation system connected to a Nu instruments Attom single-collector sector-field ICP-MS. Spot analyses were acquired using an ablation time of 12 s, a spot size of 30 µm, a repetition rate of 20 Hz, and a fluence of ~3 J/cm^2. Ablated material was carried by a 100% He gas composition in chamber before combining with a 50% argon mixture along the sample line. The following elements were measured: ^{7}Li, ^{27}Al, ^{29}Si,^{31}P, ^{35}Cl, ^{44}Ca, ^{49}Ti, ^{63}Cu, ^{88}Sr, ^{89}Y, ^{98}Mo, ^{120}Sn, ^{139}La, ^{140}Ce, ^{141}Pr, ^{146}Nd, ^{149}Sm, ^{153}Eu, ^{157}Gd, ^{163}Dy, ^{166}Er, ^{172}Yb, ^{175}Lu, ^{177}Hf, ^{181}Ta, ^{186}W, ^{206}Pb, ^{232}Th, ^{238}U. Data reduction was performed in Iolite 3 (Paton et al. 2011) using the Trace Elements Data Reduction Scheme. Ablation signals indicative of the presence of inclusions in apatite were avoided. Internal standardisation used an assumed stochiometric Ca concentration of 40.04%, and NIST610 (Jochum et al. 2005) was used as the primary reference material. Data quality was monitored using reference materials Madagascar apatite, McClure apatite, Tiago apatite and Durango apatite. Relative standard deviations are typically between 5% and 20% for elements with concentrations ≥ 1ppm, and detection limits range between 5 ppb to 2 ppm (ESM 2). Full analytical details and data tables are provided in ESM 2 and 3.

Results

Trace elements in apatite: mean values

Mean trace elemental concentrations of apatite from Sn-fertile and Sn-mineralised rocks normalised to respective mean barren values are shown in Fig. 1. Apatite in Sn-fertile rocks (Fig. 1a) show, on average, 3.3x lower Sr and 1.6x higher Y concentrations than apatite from barren intrusions, resulting in 18.6x lower Sr/Y values (mean Sr/Y = 0.04). Heavy REE are up to 3x higher in Sn-fertile apatite, whereas LREE concentrations are similar to barren values, resulting in 7.6x lower La/Yb_N values for Sn-fertile apatite (mean La/Yb_N = 2.5) compared to barren apatite (mean La/Yb_N = 18.9). In combination, these signatures appear to confirm a higher degree of fractionation for Sn-fertile intrusions. Slightly elevated Mn and Fe concentrations (enrichment factor of 1.6) as well as more pronounced negative Eu anomalies in apatite from Sn-fertile rocks (mean Eu/Eu* = 0.05) similarly point towards a higher extent of plagioclase fractionation than in barren intrusions (mean Eu/Eu* = 0.21). On the other hand, Li and Sn show the highest enrichment factors in apatite from Sn-fertile intrusions: on average, Li is 3.5x higher (mean Li = 21.1 ppm) and Sn is 16.8x higher (mean Sn = 9.6 ppm) than in apatite from barren rocks (mean Li = 6.1 ppm; mean Sn = 0.6 ppm). Mean Cu, Ga, As, Ba and W concentrations are enriched by a factor of 1.2–1.6 in apatite from Sn-fertile intrusions, and mean Pb, Th and U values are between 1.9 and 4.3x higher than in barren intrusions. No significant Ce anomaly is detected (Ce/Ce* = 1.08).

Apatite in Sn-mineralised rocks shows a general pattern of trace element depletion relative to mean barren values (Fig. 1b). This observation is consistent with Bouzari et al. (2016) and Mao et al. (2016), who found that apatite in hydrothermally altered rocks (i.e., hydrothermally altered magmatic apatite or true hydrothermal apatite) has higher Ca concentrations and lower trace element concentrations (REE, Y, Mn, Sr, Pb, Th, U) and suggested that this was due to trace element loss during the hydrothermal stage. Our compilation supports their observation for REE, Y and Mn, however mean Sr and U concentrations in apatite from Sn-mineralised rocks are indistinguishable from barren ones, and Pb and Th concentrations are 1.7 and 1.4x higher, respectively (Fig. 1b). The relative depletion of Y results in high Sr/Y ratios (mean Sr/Y = 14.5) compared to apatite from barren and Sn-fertile rocks. Overall REE slopes in apatite from Sn-mineralised intrusions are slightly steeper than in Sn-fertile rocks (mean La/Yb_N = 6.4), but La/Yb_N is 2.9x lower than in apatite from barren intrusions. Europium anomalies are weaker in apatite from Sn-mineralised rocks (Eu/Eu* = 0.88) than in apatite from barren and Sn-fertile

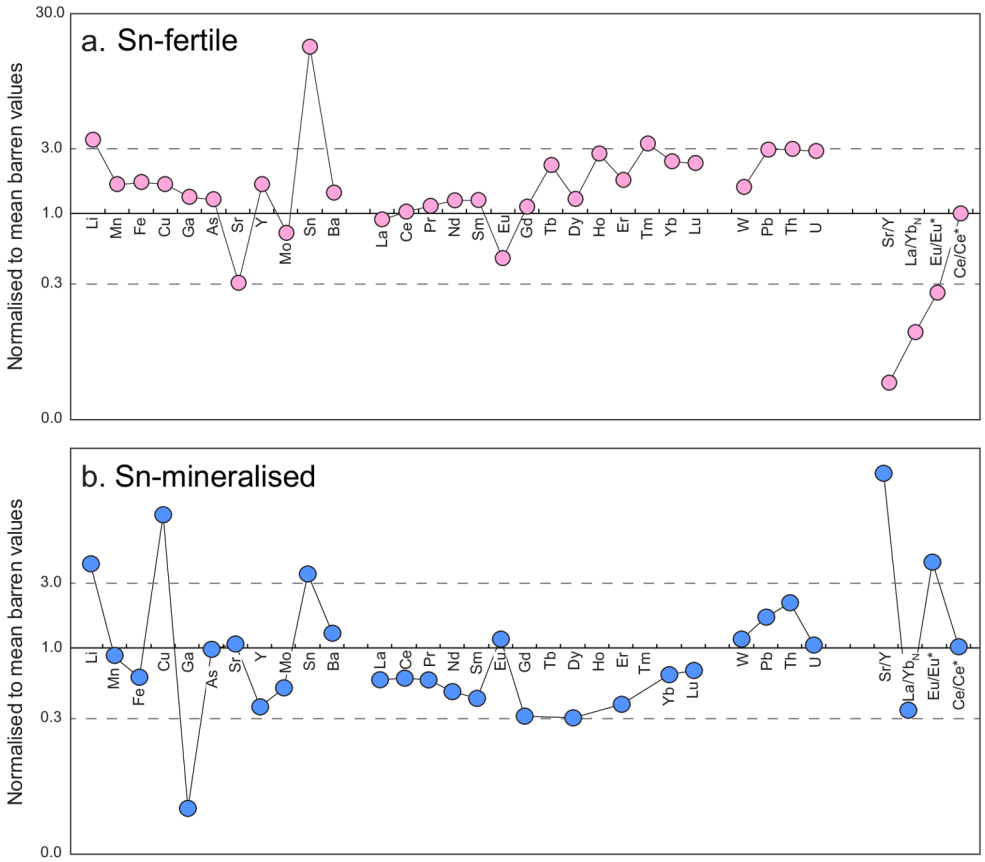

Fig. 1 Mean trace element concentrations in apatite from Sn-fertile and Sn-mineralised granitoids relative to mean concentrations of apatite from barren rocks. Data compiled from Azadbakht et al. (2018), Ge et al. (2024), Guo et al. (2022), Li et al. (2022), and this study. The most pronounced differences between barren and Sn-fertile and -mineralised lithologies are found for Li, Sn, Eu/Eu*, La/YbN, and Sr/Y, which are further examined in Figs. 2, 3 and 4

intrusions, which may indicate oxidising conditions during mineralisation (e.g., Lehmann 2021) or widespread feldspar dissolution. Consistent with Sn-fertile patterns, the most important enrichments in apatite from Sn-mineralised rocks are displayed for Li (4.1x enrichment), Sn (3.5x) and Cu (9.5x). Similar to the Sn-fertile samples, no significant Ce anomaly is observed (Ce/Ce* = 1.12).

Trace elements in apatite: data distributions

Mean concentrations can be misleading, particularly in case of skewed data distributions. Moreover, the utility of apatite as a pathfinder for tin mineralisation depends on data *ranges* (rather than means or medians) being distinguishable for different groups. In other words, a discriminant with distinct mean values but large scatter in each group is not a viable discrimination tool. For example, median Mn concentrations in apatite from barren, Sn-fertile, and Sn-mineralised rocks appear distinctive (Fig. 2a), but the data is heavily scattered for all three groups, producing widely overlapping concentration ranges. In fact, apatite from barren and Sn-fertile rocks shows almost identical upper and lower quartile ranges. As a result, if detrital apatite data were being examined with view to Sn mineralisation, Mn concentrations would not be a useful discriminant. Even apatite from Cu-fertile intrusions shows an overlapping range (yellow boxplot in Fig. 2a). A similar issue is present for La/Yb_N (Fig. 2b): while distinct mean and median values indicate that La/Yb_N in apatite is a useful tool to distinguish barren from Sn-fertile and -mineralised rocks, the range of data related to barren intrusions is large and substantially overlaps with Sn-fertile and -mineralised data, compromising its utility as a metallogenic discriminant. Better discrimination is achieved using Sr/Y (Sr shows similar results), where 75% of apatite from Sn-fertile intrusions have $Sr/Y \leq 0.029$, while 83% of barren apatite have $Sr/Y > 0.029$ (Fig. 2c; ESM 1). Tin-mineralised intrusions can also be distinguished from barren rocks using Sr/Y, as 75% of apatite

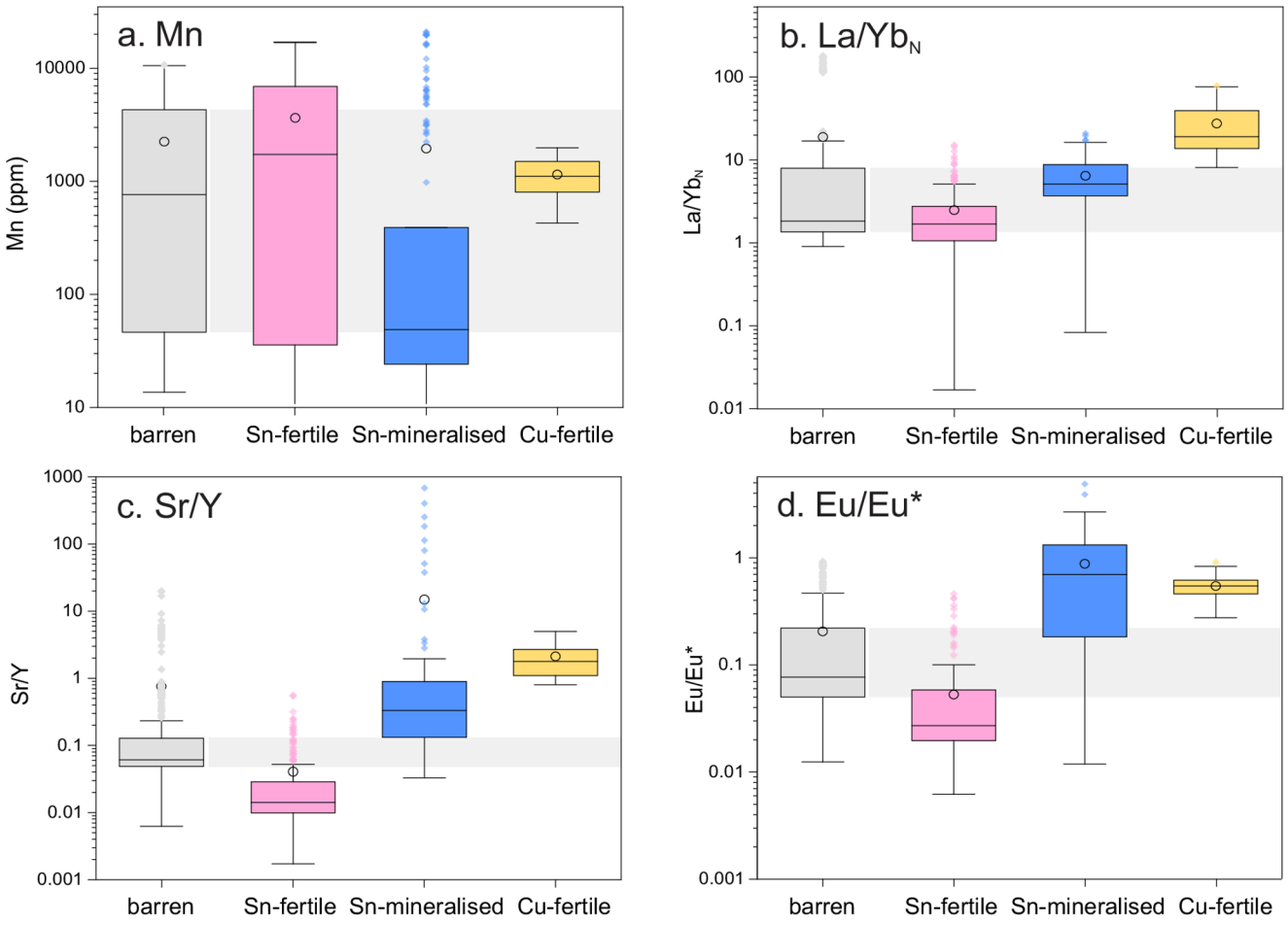

Fig. 2 Boxplots showing data distributions of four commonly used geochemical discriminants in apatite. Median (dashed lines) and mean (circles) values are distinct for apatite from barren, Sn-fertile and Sn-mineralised rocks, however their core (lower to upper quartile) ranges (boxes and grey areas) overlap significantly in many cases. This compromises the utility of Mn and La/Yb_N to fingerprint tin mineralisation. Apatite from Cu-fertile intrusions generally exhibits distinct data ranges

in Sn-mineralised rocks have Sr/Y ≥ 0.13, whereas 75% of apatite in barren intrusions have Sr/Y ratios lower than that. Europium anomalies show a similar but less clear discrimination (Fig. 2d), with apatite from Sn-fertile rocks showing generally lower values (75% show Eu/Eu* ≤0.058) than those in barren rocks (68% show Eu/Eu* >0.058), and apatite from Sn-mineralised rocks showing generally higher values (75% show Eu/Eu* ≥0.18) than barren rocks (72% show Eu/Eu* <0.18).

Our compilation shows that when entire data distributions are considered, the established discriminants Mn and La/Yb_N in apatite are unreliable pathfinders for tin mineralisation. On the other hand, Sr/Y and Eu/Eu* signatures offer more robust discrimination, even though significant overlap remains at least in the case of Eu/Eu*. Finally, we note that Sr/Y and La/Yb_N can be used to identify magmatic apatite from Cu-fertile intrusions, as both ratios are systematically higher than those of barren and Sn-fertile systems (Fig. 2b, c).

Of the geochemical proxies in apatite tested here, Sr/Y shows the most promise to distinguish between barren and Sn-fertile or -mineralised intrusions. However, plots of Sr/Y against Sn and Li (Fig. 3) illustrate how data scatter compromises its utility to fingerprint tin mineralisation. Negative correlations between Li and Sn concentrations and Sr/Y are discernible (consistent with a general trend of Li and Sn enrichment during magma fractionation), but the large scatter in Sr/Y results in significant overlap between the different groups. This compromises robust discrimination between barren, Sn-fertile and Sn-mineralised intrusions based on Sr/Y. Similar issues are observed for Mn, Fe, La/Yb_N, and Eu/Eu* (graphs in ESM1). In fact, the main reason why different types of intrusions can be distinguished in Fig. 3 is their distinct Sn and Li concentrations, which are elevated in apatite from Sn-fertile and -mineralised magmas. This warrants a closer look at Sn and Li concentrations in apatite.

In contrast to magma fractionation and redox proxies, metal concentrations in apatite directly related to tin mineralisation (Sn and Li) unambiguously distinguish between barren intrusions and those associated with tin mineralisation (Fig. 4). Specifically, Sn concentrations in apatite from Sn-fertile intrusions are consistently higher than those in barren rocks (Fig. 4a), with 75% of apatite from Sn-fertile intrusions showing Sn ≥ 1.3 ppm (maximum value: 59 ppm), whereas 97% of apatite from barren rocks show Sn < 1.3 ppm (maximum value: 1.6 ppm). Apatite from Sn-mineralised rocks also display relatively elevated tin concentrations, with 75% showing Sn ≥ 0.8 ppm, which is higher than 80% of barren apatite.

Similarly, lithium shows distinctively high concentrations in apatite from both Sn-fertile and Sn-mineralised intrusions (Fig. 4b): 75% of apatite from Sn-fertile and Sn-mineralised rocks show Li ≥ 9.7 ppm and Li ≥ 11 ppm, respectively, whereas 81% of apatite from barren intrusions have Li < 9.7 ppm. Lithium and tin concentrations are therefore the most robust geochemical discriminants to fingerprint Sn mineralisation using both magmatic and hydrothermal (or hydrothermally altered) apatite. Based on our data compilation, low Li concentrations in apatite might also be useful to identify Cu-fertile intrusions (Fig. 4b).

Discussion

Our data compilation shows patterns consistent with our current understanding of tin metallogeny: the distinctly low Sr/Y and Eu/Eu* signatures of apatite from Sn-fertile intrusions confirm that Sn mineralisation requires a high degree of fractionation and reducing conditions (Fig. 2c, d). On the other hand, elevated Sr/Y and Eu/Eu* for apatite from Sn-mineralised rocks likely reflects removal of REE, Y and other incompatible elements under more oxidising conditions during hydrothermal alteration. However, beyond these first order trends, the data scatter for traditional geochemical discriminators is large, and there remains significant overlap between barren and Sn-fertile and -mineralised rocks, in particular for Mn and La/Yb_N (Fig. 2a, b). Above all, this overlap between barren and Sn-fertile rocks suggests that extreme fractionation of reduced S-type granites (cf. Lehmann 2021) is a *necessary* but, on its own, *insufficient* condition for tin mineralisation. Beyond this observation, the scatter in each group, as well as overlaps between barren and fertile groups may be due to a number of factors, which we discuss in the following section.

Petrogenetic and metallogenic ambiguity of apatite compositions

The wide ranges of Mn, Eu/Eu*, La/Yb_N and Sr/Y in apatite are not surprising given the multitude of source rocks, magmatic conditions and processes these geochemical proxies may represent. Factors affecting the compositional variability of apatite include:

(1) *Source rocks and melt evolution histories are unique to each magmatic system.* Protoliths and melting conditions and degrees impart geochemical characteristics on a magma which may affect discriminants such as Sr/Y (Moyen 2009; Roberts et al. 2024). Similarly, the geochemical evolution of a melt is controlled by its crystallisation sequence. Since apatite reflects evolving melt composition, trace element concentrations in apatite will vary depending on primary melt composition and

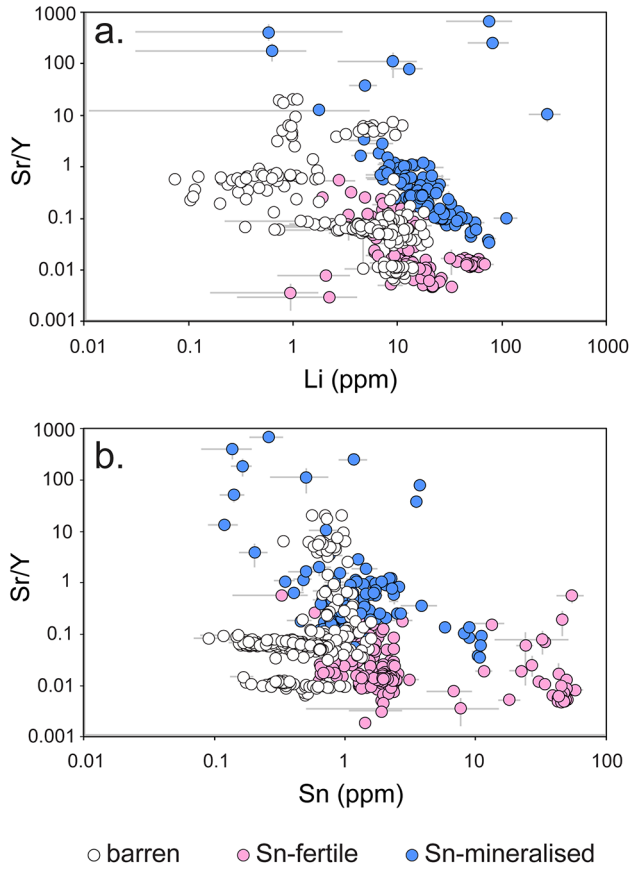

Fig. 3 Ratios of Sr/Y plotted against (**a**) Li and (**b**) Sn concentrations in apatite from our compilation. While a spurious negative correlation of Sn and Li with fractionation index Sr/Y is discernible, data scatter is large and there is significant overlap for apatite from barren, fertile and mineralised intrusions. Error bars (2SE) are only shown for our own data as uncertainties were not reported in other studies

crystallisation history (i.e., mineral phases which crystallise before or during apatite crystallisation). For example, the typical LREE depletion in apatite is controlled by crystallisation of monazite, allanite or titanite, which fractionate LREE (Tepper and Kuehner 1999; Chu et al. 2009; Miles et al. 2013; Li et al. 2022). On the other hand, trends of decreasing Y and Yb concentrations in apatite of the Criffell granitic pluton in Scotland have been interpreted to represent zircon and earlier apatite crystallisation (Miles et al. 2013). Major mineral phases may also fractionate trace elements of interest, such as amphibole or biotite (Putzolu et al. 2024). Furthermore, apatite-melt partition coefficients can vary as a function of magmatic conditions; for example, Mn partition coefficients depend on the degree of melt polymerisation (Stokes et al. 2019), and Eu partition coefficients may be influenced by redox conditions (Miles et al. 2014; Bromiley 2021). Apatite trace element compositions therefore reflect igneous processes from source to final emplacement, and they will be different for each batch of magma.

(2) *Apatite crystals do not merely record the final stages of fractionation.* Apatite often appears early in the crystallisation sequence of silicic magmas, as evidenced by their common inclusion in rock-forming minerals (e.g., biotite, feldspar and zircon; Hoskin et al. 2000; Piccoli and Candela 2002; Broska et al. 2004; Macdonald et al. 2013; Miles et al. 2013; Zhang et al. 2021; Li et al. 2022). Apatite may therefore record magma fractionation from early to late stage in any given rock sample, which will be reflected in its compositional range. This is useful to reconstruct magma petrogenesis but poses a problem from an exploration point of view: a rock from a Sn-fertile magma will likely contain apatite crystals which formed early (and long before mineralisation), and those crystals will therefore not reflect extreme fractionation; if such apatite is then analysed as a detrital grain, it will not indicate tin mineralisation using petrogenetic discriminants such as Eu/Eu*, La/Yb_N or Sr/Y.

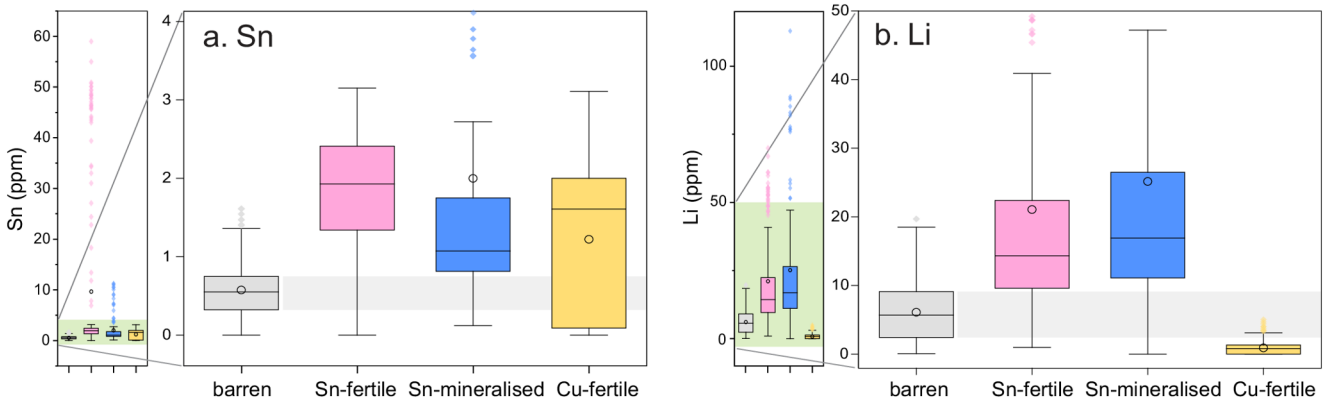

Fig. 4 Boxplots showing data distributions of Sn and Li concentrations in apatite from barren, Sn-fertile, Sn-mineralised, and Cu-fertile rocks. The core ranges (lower to upper quartile = boxes and grey areas) of Sn and Li concentrations in apatite from barren intrusions are lower than those of Sn-fertile and Sn-mineralised apatite, facilitating robust discrimination between barren granitoids and those associated with tin deposits. Our data compilation further shows that Cu-fertile intrusions are characterised by distinctively low Li concentrations in apatite

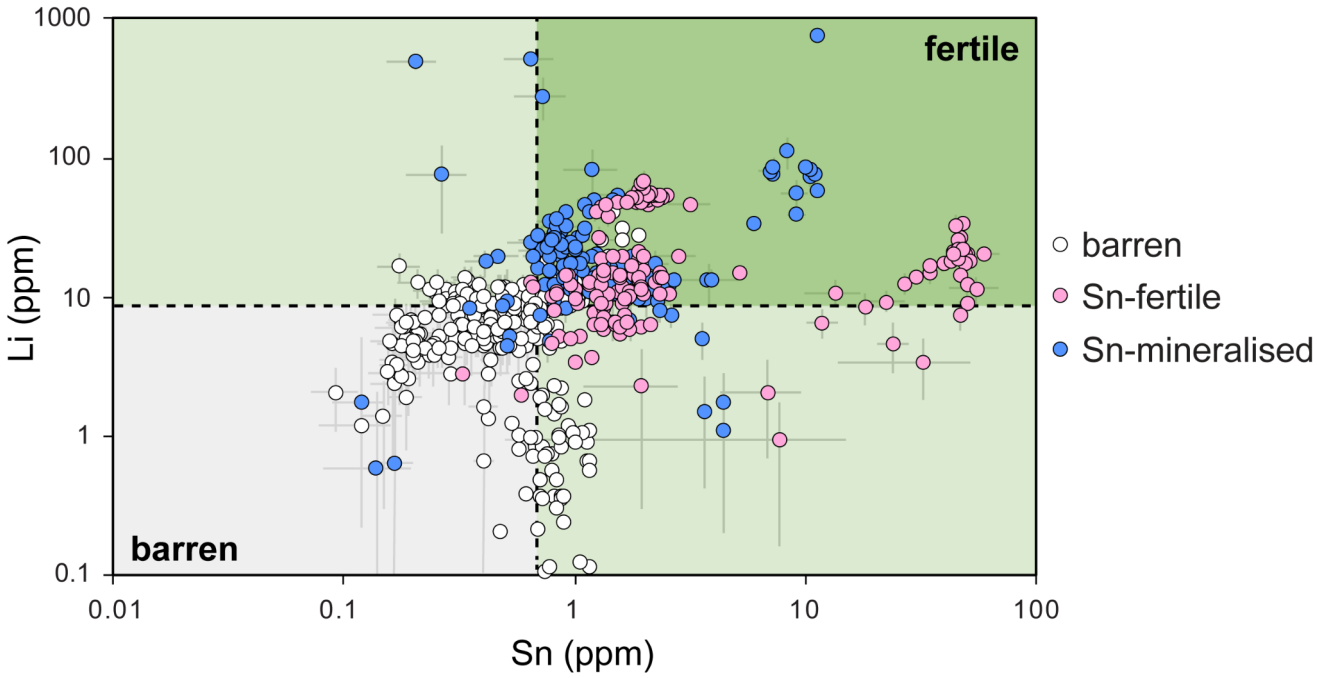

Fig. 5 Lithium and tin concentrations in magmatic apatite from barren intrusions, Sn-fertile and Sn-mineralised intrusions. 75% of apatite from barren intrusions have Li≤9.1 ppm and Sn≤0.7 ppm, while>77% of apatite from Sn-fertile and -mineralised granitoids have Li>9.1 ppm, and >82% show Sn>0.7 ppm. This demonstrates the utility of Sn and Li concentration in apatite to fingerprint tin mineralisation. Error bars (2SE) are only shown for our own data as uncertainties were not reported in other studies

(3) *Diffusion and hydrothermal alteration may modify and obscure primary trace element concentrations.* Mineral-scale diffusion (>10 µm scale) in apatite at magmatic temperatures likely operates on timescales of days to decades for many elements (Ca, Pb, Sr, Mn, U, Li, F, Cl, OH; Cherniak 2010). Diffusive re-equilibration of apatite with their host (melt or mineral) may therefore alter its trace element composition and obscure primary magmatic signatures. Similarly, fluid-moderated overprinting during and after the magmatic-hydrothermal transition may disturb or replace primary compositions. For example, Bouzari et al. (2016) found that hydrothermally altered apatite has higher Ca and lower trace element concentrations than apatite from unaltered rocks, which they attributed to trace element loss during alteration. If considered within its petrogenetic context, apatite can be an insightful tool to study these metasomatic processes (e.g., Harlov et al. 2015), but in an exploration context it adds an additional layer of complexity.

(4) *Apatite may host small inclusions of other minerals which may bias analyses*. For example, monazite and zircons inclusions are commonly observed in apatite (Tepper and Kuehner 1999; Farley and Stockli 2002). REE-rich minerals monazite and xenotime are often found as inclusions in hydrothermally altered apatite zones, where they likely formed in response to the metasomatic removal of REE from apatite (e.g., Harlov et al. 2005, 2011; Zirner et al. 2015). Larger inclusions may be avoided or detected in the ablation signal, but small, dispersed mineral or fluid inclusions may not be resolvable in the signal and bias the results.

In summary, common geochemical discriminants in apatite which empirically relate tin mineralisation to petrogenetic processes (e.g., fractionation and oxidation state) show large scatter because they record magmatic evolution over a temporal and spatial extent much beyond that of any mineralising process.

Li and Sn as robust tracers of mineralisation

We show that many common geochemical discriminants are petrogenetically ambiguous and often of limited use as discriminants for tin mineralisation. Instead, *prima facie* concentrations of Sn and Li in apatite offer a more satisfactory discrimination between barren granites and intrusions associated with Sn deposits (Figs. 3, 4 and 5). This is a somewhat surprising result considering that apatite is not a primary host for either Li or Sn, which are more likely to be fractionated by micas (Ellis et al. 2022; Putzolu et al. 2024). Furthermore, Li is known to be a fast-diffusing element in most rock-forming minerals including apatite (Audétat et al. 2018; Li et al. 2020), which may obscure primary elemental

signatures. This illustrates that Sn and Li are subject to the same processes that compromise the utility of common metallogenic indices, yet they retain distinctively elevated concentrations in apatite throughout magmatic differentiation and the magmatic-hydrothermal transition. This observation is consistent with source enrichment and elevated primary Sn and Li concentrations as crucial factors for tin mineralisation (cf. Romer and Kroner 2015, 2016). However, our data compilation cannot unambiguously resolve whether the observed elevated Sn and Li concentrations are inherited from an enriched source rock, or whether additional Sn and Li was introduced at a later stage during magma fractionation. Addressing this question requires additional constraints beyond the scope of this study, e.g., are Sn and Li incorporated into the crystal lattice of apatite, or are they hosted in micro-inclusions non-resolvable by LA-ICP-MS (see ESM 3). For the purpose of testing the utility of apatite as an exploration tool for tin mineralisation, the crucial finding is that LA-ICP-MS data for apatite from Sn-fertile and -mineralised intrusions all over the world show elevated Sn and Li concentrations.

The results of this study therefore show that Sn and Li in apatite are robust discriminants for Sn mineralisation (Fig. 5). Specifically, apatite crystals with Li > 9.1 ppm and Sn > 0.7 ppm are highly likely to stem from a Sn-fertile or Sn-mineralised intrusion: 75% of apatite from barren granitoids fall below these thresholds, whereas 77% of apatite from Sn-fertile and 83% of apatite from Sn-mineralised rocks have higher Li concentrations, and 95% of apatite from Sn-fertile and 82% of apatite from Sn-mineralised rocks have higher Sn concentrations. For the new data presented in this study, mean analytical uncertainties are 22% (2SE) for Li and 13% for Sn (ESM 2); assuming more conservative uncertainties of 30% 2SE on analytical results dilutes the significance of the Li-Sn discriminant system. Despite this, based on our data compilation, we consider Li and Sn the most meaningful pathfinders to tin mineralisation using apatite.

Conclusions

Our apatite trace element data compilation reveals large variability of widely used geochemical fractionation and redox proxies for both barren, Sn-fertile and Sn-mineralised intrusions (Fig. 2), which leads to significant overlap between the groups. These findings call into question the significance of petrogenetic indicators like Mn and La/Yb_N in tin exploration, at least for the case of apatite. Instead, our data suggests that Li and Sn in apatite are a more robust discriminant for Sn mineralisation. We therefore encourage the tin research and exploration community to exercise caution when using common petrogenetic indicators (Mn, Eu/Eu*, La/Yb_N and Sr/Y), and we instead recommend including Sn and Li in their apatite trace element analyses in order to test our findings, study implications for tin metallogeny, and enhance the utility of apatite as an indicator mineral for Sn mineralisation.

Supplementary Information The online version contains supplementary material available at https://doi.org/10.1007/s00126-025-01350-2.

Acknowledgments We thank Editor-in-Chief Bernd Lehmann for his careful handling and review of our manuscript. We further thank two anonymous reviewers whose comments helped improve the manuscript.

Author contributions All authors contributed to the study conception and design. Material preparation, data collection and analysis were performed by Simon Tapster, Nick M. W. Roberts, and Dominic Skeat. Data compilation and interpretation was conducted by Martin F. Mangler. The first draft of the manuscript was written by Martin F. Mangler and all authors commented on previous versions of the manuscript. All authors read and approved the final manuscript.

Funding MFM and NJG thank the Leverhulme Trust for support (Research Project Grant RPG-2023-210).

Data availability All data underlying this study is available in the Electronic Supplementary Material.

Declarations

Competing interest The authors declare that they have no known competing financial interests or personal relationships that could have appeared to influence the work reported in this paper.

References

Audétat A, Zhang L, Ni H (2018) Copper and Li diffusion in plagioclase, pyroxenes, olivine and apatite, and consequences for the composition of melt inclusions. Geochim Cosmochim Acta 243:99–115. https://doi.org/10.1016/j.gca.2018.09.016

Azadbakht Z, Lentz DR, McFarlane CR (2018) Apatite chemical compositions from Acadian-related granitoids of New Brunswick, Canada: implications for petrogenesis and metallogenesis. Minerals 8(12):598. https://doi.org/10.3390/min8120598

Belousova EA, Griffin WL, O'Reilly SY, Fisher NI (2002) Apatite as an indicator mineral for mineral exploration: trace-element compositions and their relationship to host rock type. J Geochem Explor 76(1):45–69. https://doi.org/10.1016/S0375-6742(02)00204-2

Blevin PL, Chappell BW (1992) The role of magma sources, oxidation states and fractionation in determining the granite metallogeny of eastern Australia. Earth Environ Sci Trans R Soc Edinb 83(1–2):305–316. https://doi.org/10.1017/S0263593300007987

Blevin PL, Chappell BW, Allen CM (1996) Intrusive metallogenic provinces in eastern Australia based on granite source and composition. Earth Environ Sci Trans R Soc Edinb 87(1–2):281–290. https://doi.org/10.1017/S0263593300006684

Bouzari F, Hart CJ, Bissig T, Barker S (2016) Hydrothermal alteration revealed by apatite luminescence and chemistry: a potential indicator mineral for exploring covered porphyry copper deposits. Econ Geol 111(6):1397–1410. https://doi.org/10.2113/econgeo.111.6.1397

Bromiley GD (2021) Do concentrations of Mn, Eu and Ce in Apatite reliably record oxygen fugacity in magmas? Lithos 384:105900. https://doi.org/10.1016/j.lithos.2020.105900

Broska I, Williams CT, Uher P, Konečný P, Leichmann J (2004) The geochemistry of phosphorus in different granite suites of the western carpathians, Slovakia: the role of apatite and P-bearing feldspar. Chem Geol 205(1–2):1–15. https://doi.org/10.1016/j.chemgeo.2003.09.004

Černý P, PL Blevin P, Cuney M, London D (2005) Granite-related ore deposits. Economic Geol 100th Anniversary Volume 337–370. https://doi.org/10.5382/AV100.12

Cherniak DJ (2010) Diffusion in accessory minerals: zircon, titanite, apatite, monazite and xenotime. Rev Mineral Geochem 72(1):827–869. https://doi.org/10.2138/rmg.2010.72.18

Chu MF, Wang KL, Griffin WL, Chung SL, O'Reilly SY, Pearson NJ, Iizuka Y (2009) Apatite composition: tracing petrogenetic processes in Transhimalayan granitoids. J Petrol 50(10):1829–1855. https://doi.org/10.1093/petrology/egp054

Ding T, Ma D, Lu J, Zhang R (2015) Apatite in granitoids related to polymetallic mineral deposits in southeastern Hunan Province, Shi–Hang zone, China: implications for petrogenesis and metallogenesis. Ore Geol Rev 69:104–117. https://doi.org/10.1016/j.oregeorev.2015.02.004

Ellis BS, Neukampf J, Bachmann O, Harris C, Forni F, Magna T, Laurent O, Ulmer P (2022) Biotite as a recorder of an exsolved Li-rich volatile phase in upper-crustal silicic magma reservoirs. Geology 50(4):481–485. https://doi.org/10.1130/G49484.1

Farley KA, Stöckli DF (2002) (U-Th)/He dating of phosphates: Apatite, monazite, and xenotime. Rev Mineral Geochem 48(1):559–577. https://doi.org/10.2138/rmg.2002.48.15

Gardiner NJ, Hawkesworth CJ, Robb LJ, Whitehouse MJ, Roberts NM, Kirkland CL, Evans NJ (2017) Contrasting granite metallogeny through the zircon record: a case study from Myanmar. Sci Rep 7(1):748. https://doi.org/10.1038/s41598-017-00832-2

Gardiner NJ, Palin RM, Koopmans L, Mangler MF, Robb LJ (2024) On tin and lithium granite systems: a crustal evolution perspective. Earth-Sci Rev 5:104947. https://doi.org/10.1016/j.earscirev.2024.104947

Ge L, Xie Q, Yan J, Huang S, Yang L, Li Q, Xie J (2024) Geochemistry of apatite from Zhuxiling tungsten deposit, eastern China: a record of magma evolution and tungsten enrichment. Solid Earth Sci 9(1):100163. https://doi.org/10.1016/j.sesci.2024.01.001

Guo J, Zhang G, Xiang L, Zhang R, Zhang L, Sun W (2022) Combined mica and apatite chemical compositions to trace magmatic-hydrothermal evolution of fertile granites in the Dachang Sn-polymetallic district, South China. Ore Geol Rev 151:105168. https://doi.org/10.1016/j.oregeorev.2022.105168

Harlov DE (2015) Apatite: a fingerprint for metasomatic processes. Elements 11(3):171–176. https://doi.org/10.2113/gselements.11.3.171

Harlov DE, Wirth R, Förster HJ (2005) An experimental study of dissolution–reprecipitation in fluorapatite: fluid infiltration and the formation of monazite. Contrib Mineral Petrol 150:268–286. https://doi.org/10.1007/s00410-005-0017-8

Harlov DE, Wirth R, Hetherington CJ (2011) Fluid-mediated partial alteration in monazite: the role of coupled dissolution–reprecipitation in element redistribution and mass transfer. Contrib Mineral Petrol 162:329–348. https://doi.org/10.1007/s00410-010-0599-7

Hopkinson TN, Harris NB, Warren CJ, Spencer CJ, Roberts NM, Horstwood MS, Parrish RR (2017) The identification and significance of pure sediment-derived granites. Earth Planet Sci Lett 467:57–63. https://doi.org/10.1016/j.epsl.2017.03.018

Hoskin PW, Kinny PD, Wyborn D, Chappell BW (2000) Identifying accessory mineral saturation during differentiation in granitoid magmas: an integrated approach. J Petrol 41(9):1365–1396. https://doi.org/10.1093/petrology/41.9.1365

Jia F, Zhang C, Liu H, Meng X, Kong Z (2020) In situ major and trace element compositions of apatite from the Yangla Skarn Cu deposit, southwest China: implications for petrogenesis and mineralization. Ore Geol Rev 127:103360. https://doi.org/10.1016/j.oregeorev.2020.103360

Jochum KP, Nohl U, Herwig K, Lammel E, Stoll B, Hofmann AW (2005) GeoReM: a new geochemical database for reference materials and isotopic standards. Geostand Geoanalytical Res 29(3):333–338. https://doi.org/10.1111/j.1751-908X.2005.tb00904.x

Lehmann B (1982) Metallogeny of tin; magmatic differentiation versus geochemical heritage. Econ Geol 77(1):50–59. https://doi.org/10.2113/gsecongeo.77.1.50

Lehmann B (2021) Formation of tin ore deposits: a reassessment. Lithos 402:105756. https://doi.org/10.1016/j.lithos.2020.105756

Li W, Chakraborty S, Nagashima K, Costa F (2020) Multicomponent diffusion of F, cl and OH in apatite with application to magma ascent rates. Earth Planet Sci Lett 550:116545. https://doi.org/10.1016/j.epsl.2020.116545

Li W, Costa F, Nagashima K (2021) Apatite crystals reveal melt volatile budgets and magma storage depths at Merapi volcano, Indonesia. J Petrol 62(4):egaa100. https://doi.org/10.1093/petrology/egaa100

Li J, Chen SY, Zhao YH (2022) Trace elements in apatite from Gejiu Sn polymetallic district: implications for petrogenesis, metallogenesis and exploration. Ore Geol Rev 145:104880. https://doi.org/10.1016/j.oregeorev.2022.104880

Lormand C, Humphreys MC, Colby DJ, Coumans JP, Chelle-Michou C, Li W (2024) Volatile budgets and evolution in porphyry-related magma systems, determined using apatite. Lithos 480:107623. https://doi.org/10.1016/j.lithos.2024.107623

Macdonald R, Bagiński B, Dzierżanowski P, Jokubauskas P (2013) Apatite-supergroup minerals in UK Palaeogene granites: composition and relationship to host-rock composition. Europ J Mineral 25(3):461–471. https://doi.org/10.1127/0935-1221/2013/0025-2291

Mao M, Rukhlov AS, Rowins SM, Spence J, Coogan LA (2016) Apatite trace element compositions: a robust new tool for mineral exploration. Econ Geol 111(5):1187–1222. https://doi.org/10.2113/econgeo.111.5.1187

Miles AJ, Graham CM, Hawkesworth CJ, Gillespie MR, Hinton RW (2013) Evidence for distinct stages of magma history recorded by the compositions of accessory apatite and zircon. Contrib Mineral Petrol 166:1–19. https://doi.org/10.1007/s00410-013-0862-9

Miles AJ, Graham CM, Hawkesworth CJ, Gillespie MR, Hinton RW, Bromiley GD (2014) Apatite: a new redox proxy for silicic

magmas? Geochim Cosmochim Acta 132:101–119. https://doi.org/10.1016/j.gca.2014.01.040
Moyen JF (2009) High Sr/Y and La/Yb ratios: the meaning of the adakitic signature. Lithos 112(3–4):556–574. https://doi.org/10.1016/j.lithos.2009.04.001
Nathwani CL, Loader MA, Wilkinson JJ, Buret Y, Sievwright RH, Hollings P (2020) Multi-stage arc magma evolution recorded by apatite in volcanic rocks. Geology 48(4):323–327. https://doi.org/10.1130/G46998.1
Pan LC, Hu RZ, Bi XW, Wang Y, Yan J (2020) Evaluating magmatic fertility of Paleo-Tethyan granitoids in eastern Tibet using apatite chemical composition and nd isotope. Ore Geol Rev 127:103757. https://doi.org/10.1016/j.oregeorev.2020.103757
Pan LC, Hu RZ, Oyebamiji A, Wu HY, Li JW, Li JX (2021) Contrasting magma compositions between Cu and au mineralized granodiorite intrusions in the Tongling ore district in South China using apatite chemical composition and Sr-Nd isotopes. Am Mineral 106(12):1873–1889. https://doi.org/10.2138/am-2021-7497
Parra-Avila LA, Hammerli J, Kemp AIS, Rohrlach B, Loucks R, Lu Y, Williams IS, Martin L, Roberts MP, Fiorentini ML (2022) The long-lived fertility signature of Cu–Au porphyry systems: insights from apatite and zircon at Tampakan, Philippines. Contrib Mineral Petrol 177(2):18. https://doi.org/10.1007/s00410-021-01878-2
Paton C, Hellstrom J, Paul B, Woodhead J, Hergt J (2011) Iolite: Freeware for the visualisation and processing of mass spectrometric data. J Anal Spectrom 26(12):2508–2518. https://doi.org/10.1039/C1JA10172B
Piccoli PM, Candela PA (2002) Apatite in igneous systems. Rev Mineral Geochem 48(1):255–292. https://doi.org/10.2138/rmg.2002.48.6
Prowatke S, Klemme S (2006) Trace element partitioning between apatite and silicate melts. Geochim Cosmochim Acta 70(17):4513–4527. https://doi.org/10.1016/j.gca.2006.06.162
Putzolu F, Seltmann R, Dolgopolova A, Armstrong RN, Shail RK, Spratt J, Buret Y, Broderick C, Brownscombe W (2024) Influence of magmatic and magmatic-hydrothermal processes on the lithium endowment of micas in the Cornubian Batholith (SW England). Min Deposita 1–22. https://doi.org/10.1007/s00126-024-01248-5
Roberts NM, Hernández-Montenegro JD, Palin RM (2024) Garnet stability during crustal melting: implications for chemical mohometry and secular change in arc magmatism and continent formation. Chem Geol 659:122142. https://doi.org/10.1016/j.chemgeo.2024.122142
Romer RL, Kroner U (2015) Sediment and weathering control on the distribution of paleozoic magmatic tin–tungsten mineralization. Min Deposita 50:327–338. https://doi.org/10.1007/s00126-014-0540-5
Romer RL, Kroner U (2016) Phanerozoic tin and tungsten mineralization—tectonic controls on the distribution of enriched protoliths and heat sources for crustal melting. Gondwana Res 31:60–95. https://doi.org/10.1016/j.gr.2015.11.002
Sha LK, Chappell BW (1999) Apatite chemical composition, determined by electron microprobe and laser-ablation inductively coupled plasma mass spectrometry, as a probe into granite petrogenesis. Geochim Cosmochim Acta 63(22):3861–3881. https://doi.org/10.1016/S0016-7037(99)00210-0
Simons B, Shail RK, Andersen JC (2016) The petrogenesis of the early Permian Variscan granites of the Cornubian Batholith: lower plate post-collisional peraluminous magmatism in the Rhenohercynian Zone of SW England. Lithos 260:76–94. https://doi.org/10.1016/j.lithos.2016.05.010
Stock MJ, Humphreys MCS, Smith VC, Isaia R, Brooker RA, Pyle DM (2018) Tracking volatile behaviour in sub-volcanic plumbing systems using apatite and glass: insights into pre-eruptive processes at Campi Flegrei, Italy. J Petrol 59(12):2463–2492. https://doi.org/10.1093/petrology/egy020
Stokes TN, Bromiley GD, Potts NJ, Saunders KE, Miles AJ (2019) The effect of melt composition and oxygen fugacity on manganese partitioning between apatite and silicate melt. Chem Geol 506:162–174. https://doi.org/10.1016/j.chemgeo.2018.12.015
Taylor RG (1979) Geology of tin deposits, Developments in Economic Geology. Elsevier, 2032 Amsterdam
Taylor JR, Wall VJ (1992) The behavior of tin in granitoid magmas. Econ Geol 87(2):403–420. https://doi.org/10.2113/gsecongeo.87.2.403
Tepper JH, Kuehner SM (1999) Complex zoning in apatite from the Idaho batholith: a record of magma mixing and intracrystalline trace element diffusion. Am Mineral 84(4):581–595. https://doi.org/10.2138/am-1999-0412
Xu J, Xia XP, Wang Q, Spencer CJ, Zhang L, Zhu X (2024) Apatite textures, elemental and isotopic compositions unmask the homogenizing process in silicic magma chambers. Geophys Res Lett 51(2): e2023GL106646. https://doi.org/10.1029/2023GL106646
Yang JH, Kang LF, Peng JT, Zhong H, Gao JF, Liu L (2018) In-situ elemental and isotopic compositions of apatite and zircon from the Shuikoushan and Xihuashan granitic plutons: implication for jurassic granitoid-related Cu-Pb-Zn and W mineralization in the Nanling Range, South China. Ore Geol Rev 93:382–403. https://doi.org/10.1016/j.oregeorev.2017.12.023
Zhang L, Chen Z, Wang F, Zhou T (2021) Apatite geochemistry as an indicator of petrogenesis and uranium fertility of granites: a case study from the Zhuguangshan batholith, South China. Ore Geol Rev 128:103886. https://doi.org/10.1016/j.oregeorev.2020.103886
Zirner AL, Marks MA, Wenzel T, Jacob DE, Markl G (2015) Rare earth elements in apatite as a monitor of magmatic and metasomatic processes: the Ilímaussaq complex, South Greenland. Lithos 228:12–22. https://doi.org/10.1016/j.lithos.2015.04.013